Molecular-orbital studies of transition- and noble-metal clusters by the self-consistent-field–$X\alpha$ scattered-wave method

R. P. Messmer and S. K. Knudson*
General Electric Corporate Research and Development, Schenectady, New York 12301

K. H. Johnson, J. B. Diamond,† and C. Y. Yang
Department of Materials Science and Engineering, Massachusetts Institute of Technology, Cambridge, Massachusetts 02139
(Received 13 October 1975)

The electronic structures of small copper, nickel, palladium, and platinum clusters having simple-cubic and cubo-octahedral geometries have been calculated, using the self-consistent-field–$X\alpha$ scattered-wave (SCF-$X\alpha$-SW) approach to molecular-orbital (MO) theory. As the cluster size and coordination number are increased, the MO results show increasing similarity to the electronic structures of the corresponding crystalline metals, with the results for 13-atom cubo-octahedral clusters exhibiting all the main features of the bulk band structures, e.g., overlap of the "d band" by the "s, p band," a sharp peak in the density of states around the Fermi level in the cases of Ni, Pd, and Pt, increasing d band width through the series Cu, Ni, Pd, and Pt, and spin polarization of the levels in the case of Ni. The calculated ionization potentials decrease gradually with increasing cluster size and for the 13-atom cubo-octahedral clusters are approximately 2 eV greater than the corresponding average bulk work functions. Localized d electron states, split off from the top and bottom of the manifold of closely spaced d levels, are also observed for the cubo-octahedral transition-metal clusters. These states have no counterparts in the bulk band structures but arise because of the finite cluster size and presence of the cluster "surface". They appear to be cluster analogs of the "surface states" postulated for crystalline transition metals and probably play an important role in the chemisorption and catalytic activities of small metal aggregates of the type utilized as the active centers of heterogeneous catalysts. The SCF-$X\alpha$-SW MO results for transition-metal clusters are critically compared with those obtained for similar clusters by the extended-Hückel (EH) and complete-neglect-of-differential-overlap (CNDO) methods. The implications of these results in surface-cluster studies of chemisorption on transition metals are discussed.

I. INTRODUCTION

The electronic structures of small transition- and noble-metal clusters less than 10 Å in size are of considerable current interest. For example, the active centers of commercial heterogeneous catalysts often consist of small metallic, bimetallic, or multimetallic clusters, typically based on Group-VIII and I*B* elements, supported on a porous refractory material such as silica or alumina.[1–3] The electronic structures of small metal clusters are also intrinsically interesting in the ways they are related to the bulk band structures and surface states of the corresponding crystalline metals.

In comparison with the large number of band-structure calculations and other theoretical studies of crystalline metals and alloys,[4,5] little fundamental work has been carried out on the electronic structures of small metallic clusters. Band theory, in its conventional form, is based on the assumptions of long-range crystalline order, Bloch's theorem, and reciprocal- or $\vec{k}$-space representation, which do not apply to small clusters, where there is at most only short-range order.

Molecular-orbital (MO) theory, on the other hand, is well suited, in principle, for describing metal-cluster electronic structure but is limited by the accuracy and practicality of available MO computational techniques. Thus far, conventional MO theory, based on representing the wave functions as linear combinations of atomic orbitals (MO-LCAO theory), has been applied exclusively in semiempirical form to transition- and noble-metal clusters. Baetzold[6] has reported semiempirical MO-LCAO calculations for Ag, Pd, Cd, Cu, and Ni clusters and for Cu-Ni and Pd-Ni bimetallic clusters, utilizing both the extended-Hückel (EH)[7] and complete-neglect-of-differential-overlap (CNDO)[8] methods. Baetzold's work includes an examination of the effects of a supporting carbon substrate on the electronic structure of a palladium cluster. Blyholder[9] has also used the CNDO method to study small nickel clusters.

Following the original EH and CNDO models of Bennett, McCarroll, and Messmer[10] for the chemisorption of first-row atoms and molecules on a graphite surface, various workers have used these methods to construct cluster models of chemisorption on transition-metal surfaces. Examples include EH calculations for hydrogen chemisorption on nickel[11] and tungsten,[12] nitrogen chemisorption on tungsten,[13] carbon monoxide chemisorption on nickel,[14] and the dissociative chemisorption of first-period diatomic molecules and ethylene on tungsten and nickel.[15] CNDO calculations for hydrogen chemisorbed on nickel clusters have also

recently been reported.[16]

It is important to assess the relative efficacies of various MO techniques in the study of elemental transition- and noble-metal clusters *per se* before attempting to investigate the interactions of such clusters with adsorbates. Therefore, in the present paper we describe the results of MO calculations for Cu, Ni, Pd, and Pt clusters obtained by the recently developed self-consistent-field–$X\alpha$ scattered-wave (SCF-$X\alpha$-SW) method[17] and compare these results to the bulk band structures and surface states of the corresponding crystalline metals. We also critically compare the SCF-$X\alpha$-SW results to those obtained for metal clusters by the EH and CNDO methods. Succeeding papers will be devoted to SCF-$X\alpha$-SW studies of chemisorption on transition-metal clusters representing small catalytic aggregates *and* the active surface sites of crystalline transition metals, and to studies of the electronic interactions between clusters and supporting environments.

II. SCF-$X\alpha$-SW METHOD

The SCF-$X\alpha$-SW approach to MO theory[17] is based on the combined use of Slater's $X\alpha$ statistical theory of exchange correlation[18] and the multiple-scattered-wave method of solving the one-electron Schrödinger equation.[19] This method has been successfully applied to a wide range of polyatomic molecules and to clusters simulating local environments in nonmetallic solids. Such applications are summarized in recent review articles.[20,21] Lithium clusters containing up to 13 atoms were the first metallic aggregates investigated by the SCF-$X\alpha$-SW technique.[22] The most significant results of the latter studies are that there is a gradual increase in binding energy per atom with increasing cluster size, and a 13-atom lithium cluster with icosahedral geometry is the most energetically stable of all the clusters considered. Because the required computation time does not increase inordinately with the number of electrons per atom, the method is ideally suited for the study of small transition- and noble-metal clusters. Preliminary examples of such applications have been described in recent publications.[23–26]

The SCF-$X\alpha$-SW formalism and computational procedures have been thoroughly documented in other publications,[17–19] so that there is no need to describe them here. In the present work, the metal atomic spheres were chosen to be contiguous and nonoverlapping (the "muffin-tin" approximation), although overlapping spheres are admissible in the theory and computational procedure.[27,28] For close-packed metal clusters of the type investigated in this paper, the muffin-tin approximation is fully satisfactory, and the orbital energies do not appreciably change with moderate amounts of sphere overlap. This is consistent with the criteria for using overlapping spheres outlined in Refs. 27 and 28.

In the application of the iterative self-consistent-field procedure to a transition-metal cluster where the density of electronic energy levels around the Fermi energy is high (see Fig. 11, for example), it is frequently necessary to repopulate the levels between successive iterations. This ensures that, in the ground-state configuration, all spin orbitals with energies below the Fermi level are fully occupied, allowing for partial occupancy only at the Fermi energy itself, and is consistent with the fact that the $X\alpha$ theory rigorously satisfies Fermi statistics.[18] Full self-consistency is typically attained for a transition- or noble-metal cluster in 20 to 30 iterations. A calculation for a Cu_{13} cluster, for example, requires approximately 2 min *per iteration* on an IBM 370/168 computer, about the same amount of computer time required in a noniterative EH-MO study of the same cluster using standard computer programs. Several EH calculations have been carried out as part of our investigation, and the results are included in this paper for a one-to-one comparison with the SCF-$X\alpha$-SW results and those of previous EH calculations for transition- and noble-metal clusters.

III. SCF-$X\alpha$-SW ORBITALS OF COPPER, NICKEL, PALLADIUM, AND PLATINUM CLUSTERS

A. Cu_8 and Ni_8

For our initial MO studies of noble- and transition-metal clusters by the SCF-$X\alpha$-SW method, we have chosen Cu_8 and Ni_8 clusters having cubic geometry, the simplest structure that has been used to characterize the dispersion and size of small catalytic particles.[29] The various parameters used in the calculations are summarized in Table I. The resulting orbital energy levels of Cu_8, for a Cu-Cu internuclear distance equal to that of bulk crystalline copper, are shown in Fig. 1(a). The total energy and kinetic energy are calculated to be $\langle E_{X\alpha}\rangle = -26\,224$ Ry and $\langle T\rangle = 26\,224$ Ry, respectively. The variation of total energy and orbital energies with internuclear distance has not been investigated for Cu_8, as it was in recent SCF-$X\alpha$-SW studies of lithium clusters.[22] However, the fact that the virial theorem is satisfied to better than one part in 10^5 suggests that Cu_8 is very close to being in an equilibrium configuration. The quantities $\langle E_{X\alpha}\rangle$ and $\langle T\rangle$ are large numbers for Cu_8, compared with the corresponding values for Li_8.[22] These quantities take on very large values for larger copper and nickel clusters and for even relatively small clusters of palladium and platinum. Our current computational procedure for evaluating total energy is not sufficiently ac-

TABLE I. Parameters used in the SCF-$X\alpha$-SW calculations for metal clusters.

	Cu_8	Ni_8	Cu_{13}	Ni_{13}	Pd_{13}	Pt_{13}
α[a]	0.707	0.709	0.707	0.709	0.702	0.693
Internuclear distance (Å)	2.54	2.49	2.54	2.49	2.74	2.77
Atomic sphere radius (Å)	1.27	1.25	1.27	1.25	1.37	1.39
Outer sphere radius (Å)	3.47	3.41	3.81	3.74	4.11	4.16

[a]These are the exchange-correlation parameters for the component atoms determined by matching the $X\alpha$ total energy of the atom to the Hartree-Fock total energy, as described in Ref. 18.

curate to justify the subtraction of two such very large total energies to obtain a reliable estimate of a small energy difference. Therefore, in the present work on noble- and transition-metal clusters we shall rely entirely on information contained in the orbital energies and wave functions.

The orbital levels of Cu_8 shown in Fig. 1(a) are labeled according to the irreducible representations of the cubic (O_h) point group. All of the levels shown are derived from the 10 3d electrons and one 4s electron of each Cu atom, plus some contribution from the Cu virtual 4p orbitals. Therefore, in the Cu_8 cluster there must be a sufficient number of valence orbitals to accommodate a total of 88 electrons. The orbital degeneracy of each a_{1g} and a_{2u} level is one, that of each e_g and e_u level is two, whereas each t_{1u}, t_{2u}, t_{1g}, and t_{2g} level is triply degenerate. Allowing for twice as many electrons per orbital because of spin degeneracy, all levels up to and including the one at -0.411 Ry labeled t_{1u} are fully occupied, resulting in zero net spin polarization for the Cu_8 cluster. The first unoccupied level is t_{2g} at -0.265 Ry. The "Fermi level," E_F, separates the filled orbitals from the empty ones.

We can characterize the complete set of Cu_8 energies shown in Fig. 1(a) as a dense band of d levels bounded above and below, respectively, by the t_{1u} level at -0.411 Ry and the a_{1g} level at -0.617 Ry, both of which are predominantly s- and p-like in character, but with some d admixture. Thus if we regard this a_{1g}-t_{1u} energy interval as the precursor of the sp band in bulk, crystalline copper,[30] then already in the Cu_8 aggregate we find that the d band is totally overlapped by the sp band, as in the solid. Even the onset of electronic excitations from the highest occupied orbitals t_{1u} and e_u to the first empty orbital t_{2g}, computed by Slater's transition-state procedure,[18] occurs in the same energy range (2.0–2.6 eV) as interband transitions which are responsible for the characteristic color of solid copper.[31] We shall have more to say about the relationships between cluster electronic structure and crystal band structure in Sec. IV A of this paper.

Contour maps for two of the orbital wave functions of Cu_8, plotted in the plane of the cube face, are provided in Fig. 2. In Fig. 2(a), we have the a_{1g} orbital corresponding to the energy level -0.533 Ry shown in Fig. 1(a). The a_{1g} wave function is normalized, and its values at the contours labeled ± 4, ± 3, ± 2, ± 1, and 0 are ± 0.076, ± 0.024, ± 0.008, ± 0.002, and 0.000, respectively, the zero value indicating a node in the wave function. The d-like nature of the a_{1g} orbital is clearly evident in the

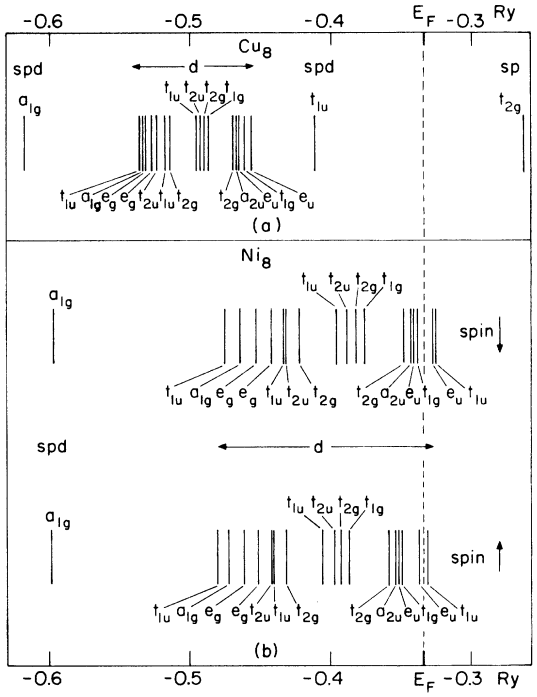

FIG. 1. (a) Electronic energy levels for a simple-cubic Cu_8 cluster, as calculated by the SCF-$X\alpha$-SW method; (b) spin-polarized electronic energy levels for a simple-cubic Ni_8 cluster, as calculated by the SCF-$X\alpha$-SW method. For each cluster, the results are shown for a nearest-neighbor internuclear distance equal to that in the corresponding bulk crystal. Levels are labeled according to the irreducible representations of the cubic (O_h) symmetry group. The "Fermi level" E_F separates the occupied levels from the unoccupied ones.

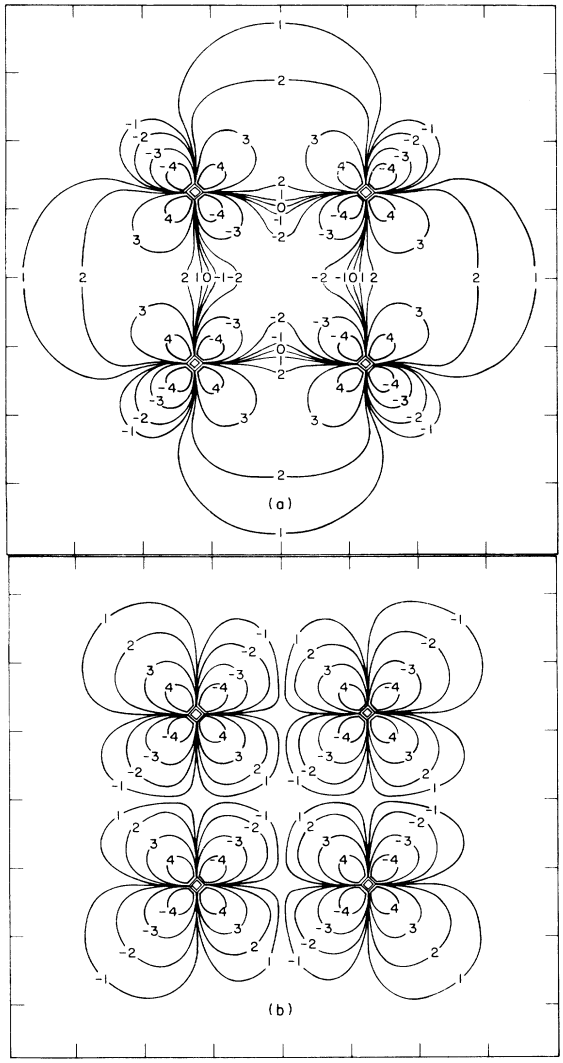

FIG. 2. Contour maps for two of the d-orbital wave functions for the simple-cubic Cu_8 cluster, plotted in the plane of a cube face. (a) a_{1g} bonding orbital corresponding to the energy level -0.533 Ry shown in Fig. 1 (a); (b) the a_{2u} antibonding orbital corresponding to the energy level -0.467 Ry shown in Fig. 1(a). Contour values decrease in absolute value with decreasing absolute values of the contour labels, the zero contour indicating a node in the wave function. Sign of the label gives the sign of the wave function.

"four-lobe" contours spreading out around each Cu nucleus. This orbital is strongly bonding in the plane of the cube face, as is indicated in Fig. 2(a) by the large amount of net wave-function overlap. The contribution of the a_{1g} orbital to bond charge density will be given by the square of the wave function. Thus Fig. 2(a) constitutes a graphic visual representation of an important part of the d-electron contribution to direct metal-metal bonding in a Cu_8 aggregate. The sp contribution to the bonding is also significant and occurs mainly through the a_{1g} orbital which is located at energy -0.617 Ry in Fig. 1(a).

The a_{2u} orbital, having the energy -0.467 Ry, is mapped in Fig. 2(b). Here the wave-function contours labeled ± 4, ± 3, ± 2, and ± 1 have the respective values of ± 0.081, ± 0.026, ± 0.008, and ± 0.003. The localized d character of this orbital is obvious from the shapes of the contours. However, in contrast to the a_{1g} bonding d orbital, a_{2u} is antibonding in the plane of the cube face in the

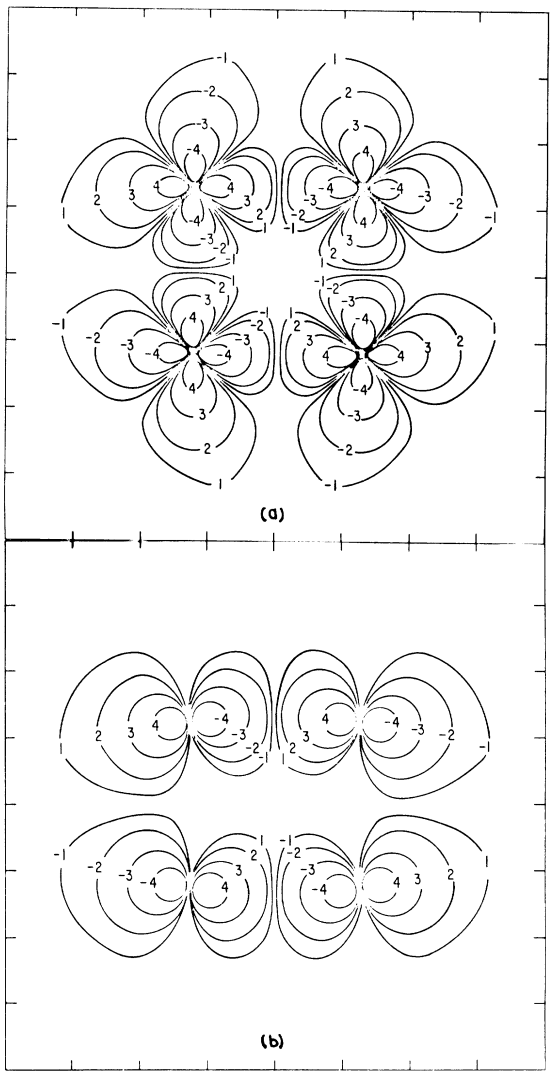

FIG. 3. Contour maps for the two highest occupied d orbitals of the simple-cubic Cu_8 cluster, plotted in the plane of a cube face. (a) The t_{1g} antibonding orbital corresponding to the energy level -0.461 Ry shown in Fig. 1(a); (b) the e_u orbital corresponding to the energy level -0.456 Ry shown in Fig. 1(a). Contour values decrease in absolute value with decreasing absolute values of the contour labels, the sign of the label giving the sign of the wave function.

sense that there is a net cancellation of positive and negative regions of the wave function, leading to effectively zero overlap. All the closely spaced d levels shown in Fig. 1(a) between -0.6 and -0.5 Ry correspond to bonding orbitals, whereas the d levels between -0.5 and -0.4 Ry correspond to nonbonding or antibonding orbitals. Contour maps of the highest occupied d orbitals, t_{1g} (-0.461 Ry) and e_u (-0.456 Ry), which are antibonding, are shown in Figs. 3(a) and 3(b), respectively.

Similar calculations by the spin-unrestricted SCF-$X\alpha$-SW technique have been carried out for the simple-cubic Ni_8 cluster, and the resulting electronic energy levels are shown in Fig. 1(b). In comparison with the Cu_8 results, the Ni_8 d band is shifted to higher energies, significantly widened, and split in energy by the net paramagnetic spin polarization, which arises because the highest occupied orbital e_u is only half filled. The "Fermi level," E_F, separates the occupied spin orbitals from the empty ones. The exchange splitting of the predominantly sp-like a_{1g} level near -0.6 Ry is considerably less than that of the levels forming the d band. The electronic structure of this "paramagnetic" Ni_8 cluster is similar to the spin-polarized band structure calculated for ferromagnetic crystalline nickel,[32] to the extent that there is overlap of the d band by the sp band and exchange splitting of the bands. However, the spin magneton number (0.25) per atom in paramagnetic Ni_8 is considerably smaller than the value (0.54) characteristic of ferromagnetic crystalline nickel. In regard to this theoretical result, it is intersting to note that Carter and Sinfelt[33] have measured the paramagnetic magneton number for small nickel crystallites and have shown that this number decreases continuously from the bulk value as the crystallite size is decreased from 100 to approximately 10 Å.

All of the atoms of Cu_8 and Ni_8 clusters are "surface" atoms, so that Fig. 1 may be interpreted as a measure of the respective "surface densities of states" of the clusters, and the orbital wave functions, such as those mapped in Figs. 2 and 3, may be interpreted as cluster "surface states." There is much current interest in the surface states of catalytic metal clusters and their relationship to the surface electronic structures of ordinary crystalline metals.[1-3] This relationship is discussed in Sec. IV B.

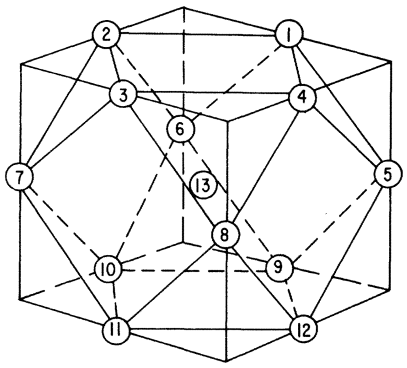

FIG. 4. Cubo-octahedral cluster containing 13 atoms.

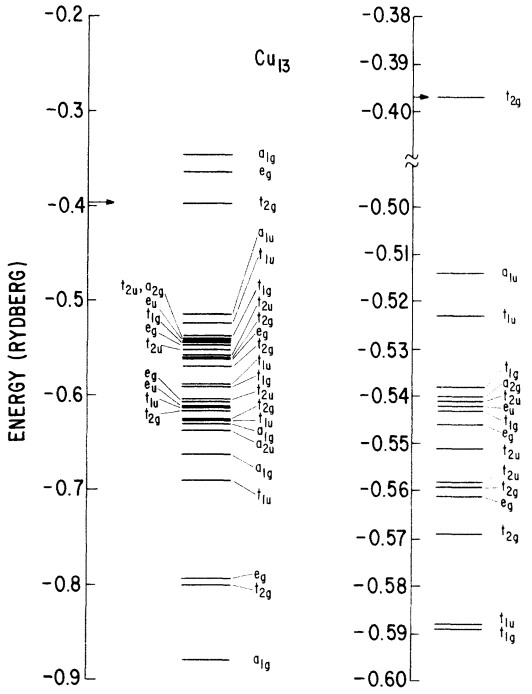

FIG. 5. SCF-$X\alpha$-SW electronic energy levels for a cubo-octahedral Cu_{13} cluster with nearest-neighbor internuclear distance equal to that for bulk crystalline copper. Levels are labeled according to the irreducible representations of the O_h symmetry group. Highest occupied level is indicated by an arrow.

B. Cu_{13}, Ni_{13}, Pd_{13}, and Pt_{13}

Similar SCF-$X\alpha$-SW calculations have been carried out for 13-atom clusters of copper, nickel, palladium, and platinum having the cubo-octahedral geometry shown in Fig. 4. This is the structure corresponding to the local arrangement of atoms in the corresponding face-centered-cubic (fcc) crystalline metals. The internuclear distances in the 13-atom clusters were constrained to the respective values of the bulk metals, as they were in the cases of Cu_8 and Ni_8. The calculational parameters are summarized in Table I.

The converged spin-restricted orbital energies for Cu_{13}, Ni_{13}, Pd_{13}, and Pt_{13} are displayed in Figs. 5, 8, 9, and 10, respectively, with the levels labeled according to the irreducible representations of the cubic (O_h) point group. On the left-

TABLE II. Energies, occupancies, and charge distributions for the occupied molecular orbitals of a cubo-octahedral Cu_{13} cluster, as determined by the SCF-$X\alpha$-SW method. Principal partial-wave components of each orbital shown in parentheses. Orbital energies in Ry. Occupancies and charges in electrons. Q (Cu-in) is the inner Cu sphere charge. Q (Cu-out) is the outer Cu sphere charge. Q (inter) is the intersphere charge. Q (extra) is the extramolecular charge.

Orbital	Energy	Occupancy	Q (Cu-in)	Q (Cu-out)	Q (inter)	Q (extra)
t_{2g} (s,p)	−0.397	5.0	2.883×10^{-2}	4.530×10^{-2}	2.904×10^{-1}	1.372×10^{-1}
a_{1u} (d)	−0.514	2.0	0.0	8.268×10^{-2}	7.882×10^{-3}	0.0
t_{1u} (s,p,d)	−0.523	6.0	1.078×10^{-2}	6.943×10^{-2}	1.145×10^{-1}	4.155×10^{-2}
t_{1g} (d)	−0.538	6.0	2.414×10^{-7}	8.097×10^{-2}	2.778×10^{-2}	5.611×10^{-4}
a_{2g} (d)	−0.540	2.0	0.0	8.163×10^{-2}	1.514×10^{-2}	5.338×10^{-3}
t_{2u} (d)	−0.541	6.0	6.073×10^{-4}	8.098×10^{-2}	1.927×10^{-2}	8.408×10^{-3}
e_u (d)	−0.542	4.0	0.0	8.101×10^{-2}	2.295×10^{-2}	4.971×10^{-3}
t_{1g} (d)	−0.543	6.0	1.409×10^{-5}	8.055×10^{-2}	2.828×10^{-2}	5.057×10^{-3}
e_g (d)	−0.546	4.0	1.202×10^{-2}	8.074×10^{-2}	1.424×10^{-2}	4.813×10^{-3}
t_{2u} (d)	−0.551	6.0	2.148×10^{-7}	8.166×10^{-2}	1.981×10^{-2}	3.070×10^{-4}
t_{2u} (d)	−0.558	6.0	1.564×10^{-3}	8.109×10^{-2}	1.849×10^{-2}	6.840×10^{-3}
t_{2g} (d)	−0.559	6.0	4.651×10^{-2}	7.699×10^{-2}	2.569×10^{-2}	3.908×10^{-3}
e_g (d)	−0.561	4.0	1.365×10^{-2}	7.834×10^{-2}	3.975×10^{-2}	6.501×10^{-3}
t_{2g} (d)	−0.569	6.0	4.967×10^{-3}	7.959×10^{-2}	3.594×10^{-2}	4.019×10^{-3}
t_{1u} (s,p,d)	−0.588	6.0	3.578×10^{-4}	7.842×10^{-2}	5.089×10^{-2}	7.714×10^{-3}
t_{1g} (d)	−0.589	6.0	3.378×10^{-4}	8.112×10^{-2}	2.431×10^{-2}	1.896×10^{-3}
t_{2u} (d)	−0.603	6.0	4.113×10^{-5}	7.909×10^{-2}	4.930×10^{-2}	1.629×10^{-3}
e_g (d)	−0.606	4.0	7.818×10^{-2}	7.201×10^{-2}	5.745×10^{-2}	2.615×10^{-4}
e_u (d)	−0.611	4.0	0.0	8.002×10^{-2}	3.852×10^{-2}	1.214×10^{-3}
t_{1u} (s,p,d)	−0.611	6.0	9.597×10^{-3}	7.552×10^{-2}	7.804×10^{-2}	6.069×10^{-3}
t_{2g} (d)	−0.616	6.0	4.919×10^{-2}	7.627×10^{-2}	3.506×10^{-2}	5.046×10^{-4}
t_{2g} (d)	−0.625	6.0	6.784×10^{-3}	7.659×10^{-2}	7.066×10^{-2}	3.442×10^{-3}
t_{1u} (s,p,d)	−0.626	6.0	3.684×10^{-3}	7.771×10^{-2}	6.157×10^{-2}	2.279×10^{-3}
a_{1g} (s,p,d)	−0.630	2.0	1.050×10^{-3}	7.438×10^{-2}	9.920×10^{-2}	7.216×10^{-3}
a_{2u} (d)	−0.636	2.0	1.942×10^{-3}	7.971×10^{-2}	3.820×10^{-2}	3.291×10^{-3}
a_{1g} (s,p,d)	−0.662	2.0	1.626×10^{-2}	6.873×10^{-2}	1.454×10^{-1}	1.362×10^{-2}
t_{1u} (s,p,d)	−0.689	6.0	7.005×10^{-2}	5.649×10^{-2}	2.328×10^{-1}	1.930×10^{-2}
e_g (d)	−0.793	4.0	8.520×10^{-1}	8.107×10^{-3}	5.039×10^{-2}	3.662×10^{-4}
t_{2g} (d)	−0.800	6.0	8.375×10^{-1}	1.010×10^{-2}	4.063×10^{-2}	6.949×10^{-4}
a_{1g} (s,p)	−0.879	2.0	2.810×10^{-1}	3.739×10^{-2}	2.621×10^{-1}	8.313×10^{-3}
$3p$ (Cu-out)	−5.409	72.0	0.0	8.333×10^{-2}	0.0	0.0
$3p$ (Cu-in)	−5.587	6.0	1.000	0.0	0.0	0.0
$3s$ (Cu-out)	−8.309	24.0	0.0	8.333×10^{-2}	0.0	0.0
$3s$ (Cu-in)	−8.484	2.0	1.000	0.0	0.0	0.0

hand side of each figure, we show the entire energy range bracketing the band of closely spaced d levels and the overlapping s,p levels. An arrow points to the highest occupied level in each case. On the right-hand side of each figure, the highest occupied and lowest unoccupied levels are shown on a much finer energy mesh in order to resolve the ordering of orbital states around the Fermi energy (indicated by an arrow).

For example, in the case of Cu_{13} (Fig. 5), the closely spaced levels in the energy range between −0.5 and −0.7 Ry correspond to predominantly d-like orbitals, whereas the a_{1g} (−0.879 Ry) and t_{2g} (−0.397 Ry) levels correspond to predominantly s,p-like orbitals. In Table II, we list the principal partial-wave components, energies, occupancies, and charge distributions of all the occupied orbitals of Cu_{13} shown in Fig. 5. The distribution of orbital charges among the various regions of the cluster is especially interesting, indicating that some orbitals, such as t_{2g} (−0.559 Ry), are delocalized throughout the cluster, while other orbitals, such as a_{2g} (−0.540 Ry), are automatically excluded from the central or inner atomic sphere by symmetry restrictions and therefore are associated exclusively with the outer atoms. Such considerations are helpful in differentiating between "bulk" and "surface" contributions to the electronic structure of metal clusters and their relationship to the bulk and surface properties of crystalline metals (see Sec. IV). As in the previously described results for Cu_8, an analysis of the computed wave functions indicates that most of the orbitals near the bottom of the d band in Cu_{13} are bonding, whereas most of the orbitals near the top of the d band are antibonding

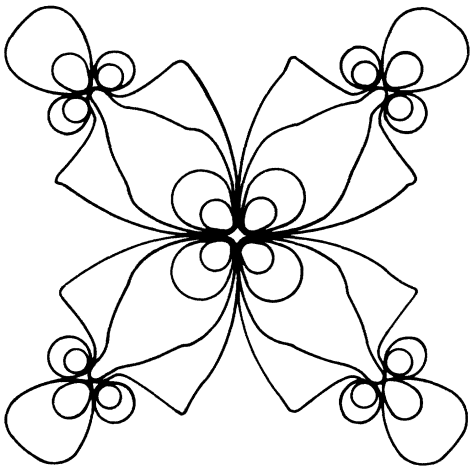

FIG. 6. Contour map for the t_{2g} bonding d orbital of Cu_{13} corresponding to the energy level -0.800 Ry shown in Fig. 5, plotted in the equatorial plane containing atoms 5–8, and 13 of the cubo-octahedron illustrated in Fig. 4.

or nonbonding. The two energy levels, t_{2g} (-0.800 Ry) and e_g (-0.793 Ry), which are located well below the manifold of closely spaced d levels in Cu_{13}, also correspond to d orbitals which are bonding between the central atom and outer atoms of the cubo-octahedron, but which are primarily localized on the central atom (see Table II). Contour maps for these orbitals, plotted in a plane passing through the central atom and four outer atoms of the cubo-octahedron (the atoms labeled 13 and 5–8 in Fig. 4), are shown in Figs. 6 and 7, respectively. While the main band of d levels in Cu_{13} corresponds closely to the d band characteristic of bulk, crystalline copper (see Sec. IV A), the two deep-lying d levels, t_{2g} (-0.800 Ry) and e_g (-0.793 Ry), have no close counterpart in bulk copper and are artifacts of the deeper potential energy of the central atom of Cu_{13}, compared with the outer of "surface" atoms of the cluster, attained at self-consistency.

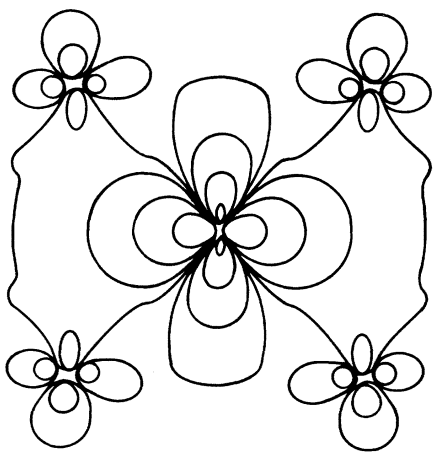

FIG. 7. Contour map for the e_g bonding d orbital of Cu_{13} corresponding to the energy level -0.793 Ry shown in Fig. 5, plotted in the equatorial plane containing atoms 5–8, and 13 of the cubo-octahedron illustrated in Fig. 4.

A comparison of Figs. 8–10 with Fig. 5 reveals some gross similarities among the energy levels of Ni_{13}, Pd_{13}, and Pt_{13} and those of Cu_{13}, particularly in regard to the ordering of orbital states. There are, however, important differences with respect to orbital occupancy and bandwidth. In Cu_{13}, the d band lies well below the highest occupied level, t_{2g} (-0.397 Ry), a rather spatially diffuse s,p-like orbital. On the other hand, in each of the clusters, Ni_{13}, Pd_{13}, and Pt_{13}, the Fermi level runs through the top of the d band, where the density of states is high. Thus in Cu_{13}, the d-band orbitals are completely occupied by electrons, while in Ni_{13}, Pd_{13}, and Pt_{13}, the topmost d orbital a_{1u} is unoccupied.

Only in the case of Ni_{13} are the highest t_{1g} and t_{1u} energy levels, corresponding, respectively, to a pure d orbital and "hybrid" s, p, d orbital, practically degenerate (at energy -0.412 Ry), imply-

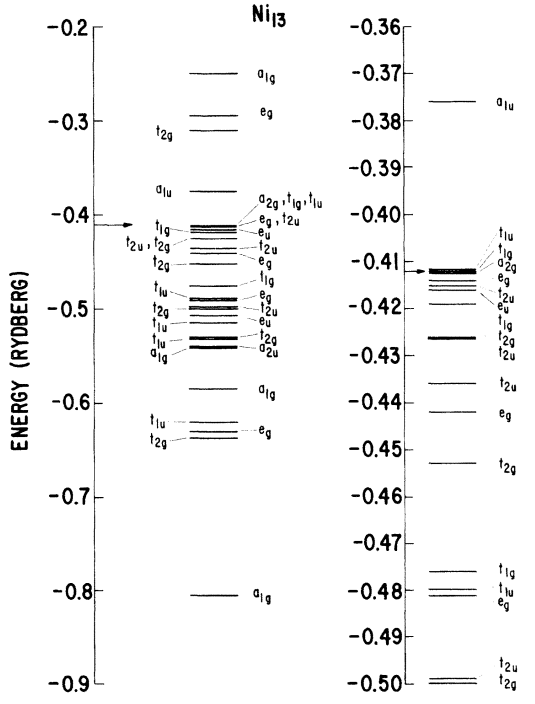

FIG. 8. SCF-$X\alpha$-SW electronic energy levels for a cubo-octahedral Ni_{13} cluster with nearest-neighbor internuclear distance equal to that for bulk crystalline nickel. Levels are labeled according to the irreducible representations of the O_h symmetry group. Highest occupied level is indicated by an arrow.

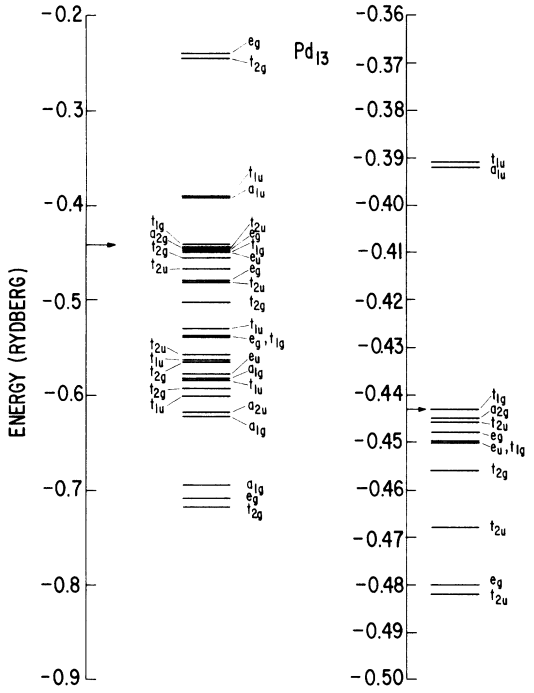

FIG. 9. SCF-$X\alpha$-SW electronic energy levels for a cubo-octahedral Pd_{13} cluster with nearest-neighbor internuclear distance equal to that for bulk crystalline palladium. Levels are labeled according to the irreducible representations of the O_h symmetry group. Highest occupied level is indicated by an arrow.

ing that the levels are half filled with three electrons each. Attempts to occupy one of these orbitals with its full complement of six electrons, leaving the other orbital empty, resulted in oscillations of the ordering of these nearly degenerate levels with respect to the Fermi energy during the iterative procedure. Thus, applying Hund's rules to the orbital occupancy in Ni_{13}, we find that there are six unpaired spins, leading to a net spin polarization and paramagnetism of the cluster. Note that in the Pd_{13} and Pt_{13} clusters, the highest t_{1u} (s, p, d) orbital is not degenerate with the highest t_{1g} (d) orbital, but is closer in energy to the empty a_{1u} (d) orbital. Hence in Pd_{13} and Pt_{13} it is possible to obtain a convergent solution with the topmost t_{1g} (d) orbital fully occupied with six spin-paired electrons, resulting in no net spin polarization or magnetism for these clusters.

Since Ni_{13} is paramagnetic, a more accurate representation of the electronic structure can be obtained by carrying out the SCF-$X\alpha$-SW calculations in a spin-unrestricted fashion, allowing different molecular orbitals for different spins, as was done in the case of Ni_8 [cf. Fig. 1(b)]. The results of such a calculation are shown in Fig. 11. Like the spin-restricted results for Ni_{13} shown in Fig. 8, the spin-polarized energy levels in Fig. 11 are displayed on two energy scales, one encompassing the entire d band and overlapping s, p levels, and the other resolving the upper part of the d band on a much finer energy mesh. The "Fermi level," E_F, separates the unoccupied spin orbitals from the occupied ones. Note that the spin splitting of the energy levels corresponding to orbitals which are predominantly s, p-like is somewhat smaller than that of the d levels. The spin magneton number per atom in Ni_{13} is 0.46, assuming the net spin density, arising from the six unpaired spins in the topmost occupied $t_{1u}\uparrow$ (−0.425 Ry) and $t_{1g}\uparrow$ (−0.427 Ry) spin-orbittals, to be delocalized uniformly over all 13 atoms. This value may be compared with the magneton number (0.25) per atom calculated for the smaller cluster, Ni_8. Although we have considered nickel clusters of only two different sizes and geometries in the present paper, these results are consistent with the experimental observation of Carter and Sinfelt[33] that the paramagnetic magneton number for small nickel crystallites decreases continuously from the bulk value as the crystallite size is reduced from 100 to approximately 10 Å.

A comparison of Fig. 8 (or Fig. 11) with Figs. 9 and 10 reveals a systematic trend of increasing d bandwidth and relative spacing between the en-

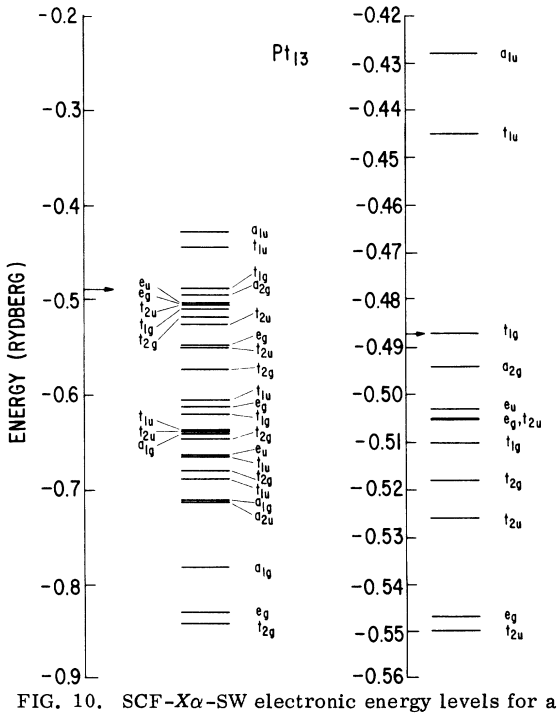

FIG. 10. SCF-$X\alpha$-SW electronic energy levels for a cubo-octahedral Pt_{13} cluster with nearest-neighbor internuclear distance equal to that for bulk crystalline platinum. Levels are labeled according to the irreducible representations of the O_h symmetry group. Highest occupied level is indicated by an arrow.

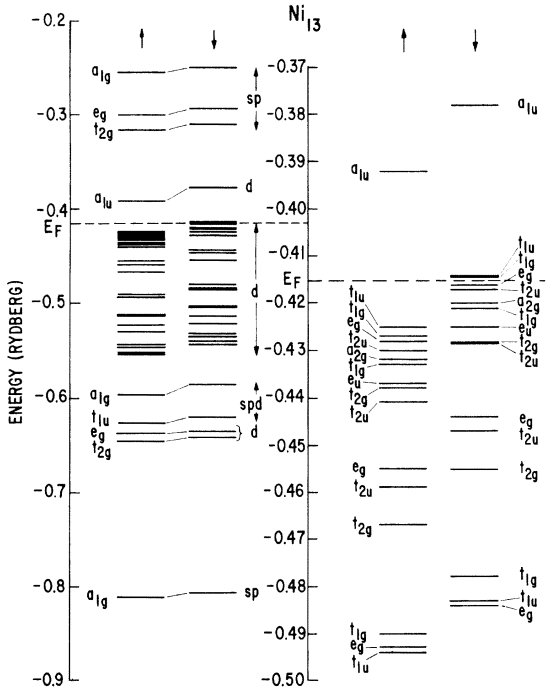

FIG. 11. Spin-polarized SCF-$X\alpha$-SW electronic energy levels for a cubo-octahedral Ni_{13} cluster with nearest-neighbor internuclear distance equal to that for bulk crystalline nickel. Levels are labeled according to the irreducible representations of the O_h symmetry group. "Fermi level" E_F separates the occupied levels from the unoccupied ones.

ergy levels through the series Ni_{13}, Pd_{13}, and Pt_{13}, while largely preserving the ordering of orbital symmetries. As a result, the density of states around the Fermi level, while high in all three clusters, decreases and broadens somewhat as one progresses from Ni_{13} to Pd_{13} and Pt_{13}. Ni_{13}, Pd_{13}, Pt_{13} all have the same number of valence electrons as well as geometry, yet the calculations predict that only Ni_{13} is magnetic, which is consistent with the situation in the bulk. These trends correspond rather remarkably to trends in the electronic band structure and density of states for the corresponding bulk crystalline solids. Section IV is devoted to a direct comparison of the cluster electronic structures with the densities of states for the crystalline metals, including a discussion of how cluster molecular orbitals can be used to describe surface electronic states.

IV. COMPARISON OF CLUSTER AND CRYSTAL ELECTRONIC STRUCTURE

A. Bulk densities of states

In Fig. 12 is a comparison of the occupied orbital energy levels of cubic Cu_8 and cubo-octahedral Cu_{13}, as described in Sec. III, with the density of occupied states for bulk crystalline copper, as calculated by Janak *et al.*[34] using the SCF-$X\alpha$ Korringa-Kohn-Rostoker (KKR)[35] band-structure method. Also included for comparison are the occupied orbital energies for a Cu_2 molecule with internuclear distance equal to that of bulk copper, as determined by the SCF-$X\alpha$-SW technique, and the SCF-$X\alpha$ energy levels of the isolated Cu atom in two alternative electron configurations. The approximations made in the SCF-$X\alpha$-KKR approach to crystalline band structure are very similar to those used in the SCF-$X\alpha$-SW molecular-orbital theory,[17] so that the comparison in Fig. 12 is a truly consistent one. Since the zero of energy in a band-structure calculation is an arbitrary one, the density of states for bulk copper has been arbitrarily shifted in Fig. 12 so as to roughly align the top of the d band with the corresponding levels for the Cu_{13} cluster.

The overall downward shift of the calculated d-like energy levels from Cu_2 to Cu_{13} in Fig. 12 may at first seem strange, but when one recalls that these are orbital energies and not "transition-state" energies[18] this shift can be easily understood. It is the transition-state energies which represent ionization potentials and thus can be compared directly with photoelectron spectra. However, we have found that for a given metal cluster, the effect of carrying out a transition-state calculation is to give a set of energy levels that differ from the unrelaxed orbital energies by an almost constant shift of all the orbitals to lower energy. The orbital relaxation decreases with increasing cluster size, approaching zero in the limit of the infinite crystal, where the molecular orbitals become Bloch states.[18] Thus the relative shifts of the d bands seen in Fig. 12 as one pro-

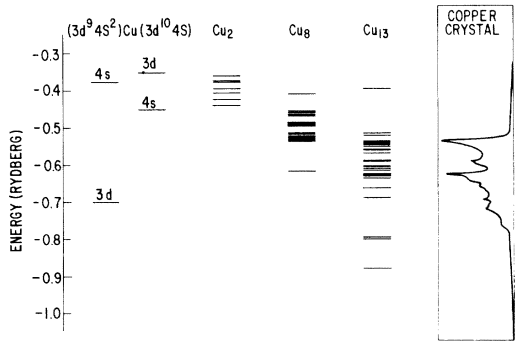

FIG. 12. Comparison of the occupied SCF-$X\alpha$-SW electronic energy levels for Cu_2, Cu_8, and Cu_{13} with the electronic density of states for bulk crystalline copper calculated by SCF-$X\alpha$-KKR band-structure theory (Ref. 34). For the sake of comparison, the latter has been adjusted so that the Fermi levels of the crystal and Cu_{13} cluster approximately coincide. Also shown for comparison are the SCF-$X\alpha$ energy levels of the isolated Cu atom for two different electronic configurations.

gresses from Cu_2 to Cu_{13} will be partially compensated for if transition-state energies, rather than unrelaxed orbital energies, are shown. Actual transition-state calculations for the highest occupied orbitals of the clusters lead to ionization potentials of 7.8 and 7.3 eV for Cu_8 and Cu_{13}, respectively. These quantities may be compared with the work function, 4.7 eV, of bulk copper.

The density of states for bulk copper shown in Fig. 12 is in good agreement with the principal emission peaks and bandwidth associated with the d-band ultraviolet photoelectron spectrum (UPS) of bulk copper.[34] The clustering of the energy levels and the total bandwidth of d orbitals in Cu_{13}, as shown in Fig. 12, closely match the main features of the d-band density of states for bulk copper. Even the more delocalized s, p-like orbitals of Cu_{13}, which correspond to the lowest and highest occupied energy levels shown in Fig. 12 (see also Fig. 5), have a one-to-one correspondence to the delocalized s, p-like Bloch conduction-band states of crystalline copper. The latter states are responsible for the low-density tails in the density of states for bulk copper shown in Fig. 12 at energies below and above the main d-band peaks. The energy for electronic transitions between the top of the manifold of closely spaced d levels of Cu_{13} and unoccupied s, p levels just above the Fermi energy is very close to the value (~ 2 eV) for the onset of transitions between the d band and conduction band responsible for the color of bulk copper.[31]

These results strongly suggest that short-range order, as represented by the 13-atom cubo-octahedral cluster, determines the principal features of the band structure for crystalline copper. It should be noted, however, that the two main peaks in the density of states of bulk copper do not correspond respectively to t_{2g}- and e_g-like bands of d orbitals, as sometimes suggested in the literature, but rather to groups of orbitals of mixed symmetries. From what has been said in Sec. III about the bonding character of the Cu_{13} orbitals, it is reasonable to think of the lower-energy d-band peak in the density of states of bulk copper as corresponding to orbitals that are predominantly bonding, whereas the d-band peak closest in energy to the Fermi level may be thought of as corresponding to orbitals that are antibonding and nonbonding.

At this point, it is appropriate to point out the work of House and Smith[36] and Keller,[37] who have compared the electronic densities of states of small copper clusters with those of bulk copper, using a muffin-tin formalism somewhat similar to the scattered-wave method employed in the present paper. Their approach, however, is non-self-consistent and completely avoids the calculation of discrete molecular orbitals, focusing instead on the direct determination of density-of-states profiles for the clusters. Although there is some similarity between the results of House and Smith[36] for Cu_{13} and the density of states for bulk copper, the details are lacking and no orbital interpretation of the cluster electronic structure is provided.

One can generate density-of-states profiles for metal clusters which permit a one-to-one comparison with bulk densities of states, without sacrificing the molecular-orbital interpretation, by "broadening" the discrete eigenvalue spectrum with a set of Gaussian functions yielding a density-of-states function of the form

$$N(\epsilon) = \sum_i \frac{n_i}{(2\pi\sigma)^{1/2}} \exp\left(-\frac{(\epsilon-\epsilon_i)^2}{2\sigma^2}\right). \quad (1)$$

In this expression, ϵ_i is the orbital eigenvalue, n_i is the orbital occupation number, and σ is an appropriately chosen broadening parameter. This procedure may also be interpreted as simulating the effect of adding more shells of atoms to the cluster, namely, the insertion of many new eigenvalues between the already closely spaced energy levels, although it preserves the spectral density and width of the d-band characteristic of the small cluster.

We have applied the above expression to the SCF-$X\alpha$-SW orbital spectrum of the cubo-octahedral Ni_{13} cluster shown in Fig. 8 for a broadening parameter, $\sigma = 0.01$ Ry, chosen to give sufficient resolution of structure. The resulting density-of-states profile for Ni_{13} is shown in Fig. 13. For comparison, the majority-spin density of states for crystalline nickel, calculated by Callaway and Wang[32] with an SCF-$X\alpha$-LCAO band-structure method, is also shown in Fig. 13. The correspondence between the results for the cluster and those for the crystal is rather good, especially in regard to the fact that in both cases the Fermi energy intersects the top of the d band where the density of states is sharply peaked. This may be compared with the results obtained for Cu_{13} and bulk copper (see Fig. 12), where the d band is completely filled and lies well below the Fermi level, which intersects a low-density region of predominantly s,p-like states. The molecular orbitals of Ni_{13} that correspond to the sharp peak in the density of states near the Fermi level (cf. Figs. 8 and 13) are principally antibonding and nonbonding d orbitals, whereas the Ni_{13} d orbitals that correspond to the broad peak centered around 0.1 Ry in Fig. 13 are largely bonding. The Ni_{13} peak near 0.25 Ry in Fig. 13 also corresponds to bonding d orbitals, but predominantly ones of t_{2g} and e_g symmetry that are localized primarily on the central atom of the cubo-octahedron (cf. Fig. 8). The Ni_{13} peak near 0.4 Ry in Fig. 13 is due to

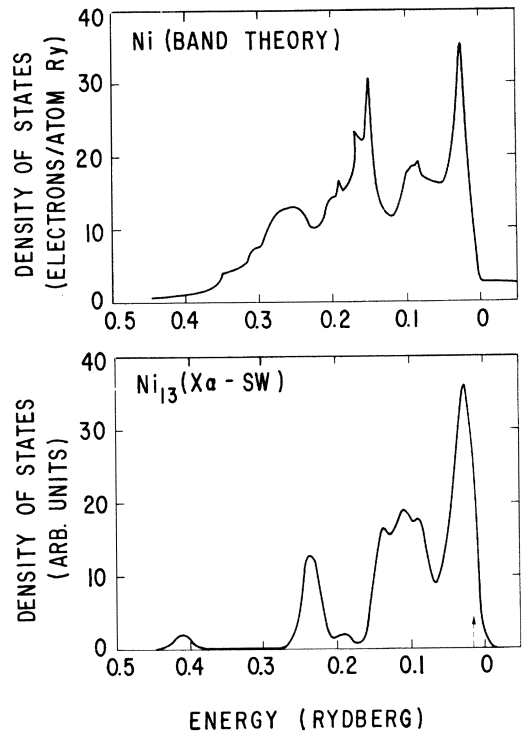

FIG. 13. Comparison of the majority-spin electronic density of states for bulk crystalline nickel, calculated by the SCF-$X\alpha$-LCAO method (Ref. 32) with the "density of states" for a cubo-octahedral Ni_{13} cluster based on the Gaussian-broadened SCF-$X\alpha$-SW energy levels shown in Fig. 8.

the strongly bonding s,p-like a_{1g} orbital, the state having the lowest energy level shown in Fig. 8.

Densities of states for the cubo-octahedral Pd_{13} and Pt_{13} clusters, based on the orbital eigenvalues shown in Figs. 9 and 10, have also been generated, and the resulting density-of-state profiles are displayed in Fig. 14. The principal structural features of these profiles are very similar to those for Ni_{13}, for example, the presence of a sharp peak in the density of states around the Fermi energy. However, this peak broadens and the total bandwidth of the density of states increases through the series Ni_{13}, Pd_{13}, and Pt_{13}. This trend matches the one for the densities of states of the corresponding bulk crystalline metals, as revealed by x-ray photoelectron spectra.[38]

Differences between the cluster and crystal densities of states (e.g., see Fig. 13) are due, in part, to the effects of long-range crystalline order. Furthermore, contributions of the cluster "surfaces" automatically show up in the electronic structures of Ni_{13}, Pd_{13}, and Pt_{13}, whereas band-structure calculations for the bulk metals normally avoid surface effects through the imposition of cyclic boundary conditions. The possible relevance of cluster calculations to the surface electronic structures of noble and transition metals is discussed in Sec. IV B.

B. Surface electronic structure

It has been known for some time that electrons can exist in states localized near the surface of a crystal.[25,39] Most attention has been focused on the intrinsic surface states of semiconductors because of their effects on the properties of solid-state devices.[39,40] More recently, the existence of surface states on crystalline noble and transition metals has been the subject of considerable speculation,[41–44] stimulated in part by the apparent sensitivity of ultraviolet photoelectron spectra[45,46] and catalytic activity[47] to surface conditions.

On the other hand, the catalytic properties of small transition-metal clusters (less than 10 Å in diameter) of the type which constitute the active centers of commercial heterogeneous catalysts are often quite different from those characteristic of crystalline transition-metal surfaces.[1–3] Therefore, it is important to establish whether the concept of a "surface state" is meaningful in the limit of a small transition-metal cluster and whether the electronic structures of such clusters

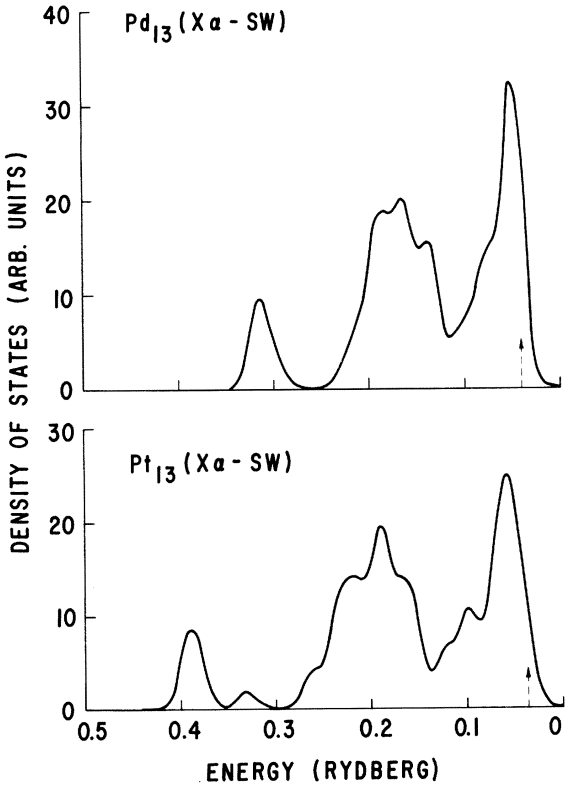

FIG. 14. Electronic "densities of states" for cubo-octahedral Pd_{13} and Pt_{13} clusters based on the Gaussian broadened SCF-$X\alpha$-SW energy levels shown in Figs. 9 and 10, respectively.

are relevant to the surface states of single-crystal or polycrystalline transition metals. Since chemisorption is a precursor of catalysis, the relationship of chemisorption activity to surface states, on both small clusters and crystalline surfaces, is also of fundamental importance.[24,48]

The 13-atom cubo-octahedral clusters considered in this paper are particularly useful for investigating these issues. First of all, the MO representation of electronic wave functions and the utilization of orbital symmetries immediately allow one to distinguish between those orbitals which have no components on the central atom of the cubo-octahedron and which therefore are localized on the 12 equivalent "surface" atoms (hereafter called "surface orbitals"), and those orbitals which have components on all 13 atoms or are predominantly localized on the central atom (hereafter called "bulk orbitals"). Obviously, the distinction between "surface" and "bulk" states for such small clusters is academic since most of the atoms are actually surface atoms. Nevertheless, we shall adopt this terminology because it allows one to construct simple cluster analogs for the bulk and surface states of crystals entirely within the framework of "real-space" SCF-$X\alpha$ MO theory, thereby circumventing the conceptual and computational problems associated with the representation of localized surface states on semi-infinite solids from the point of view of delocalized band-structure theory and "$\vec{k}$-space" concepts.[41-43] Indeed, the rotational equivalence of the surface atoms of the cubo-octahedron is analogous to the translational equivalence of the surface atoms on an fcc crystal. However, the cubo-octahedral cluster includes both (100) and (111) type surface planes (see Fig. 4), so that this cluster is actually analogous to a faceted or polycrystalline surface, rather than a single-crystal one.

Using the orbital symmetries associated with the electronic energy levels of Cu_{13} and Ni_{13} shown in Figs. 5 and 8, we can separate the "bulk" and "surface" orbitals, resulting in the energy level diagrams shown in Fig. 15. The first thing to note is the high density of surface orbitals in the vicinity of the Fermi level in the case of Ni_{13}. These are antibonding and nonbonding d orbitals which are spatially oriented away from the surface

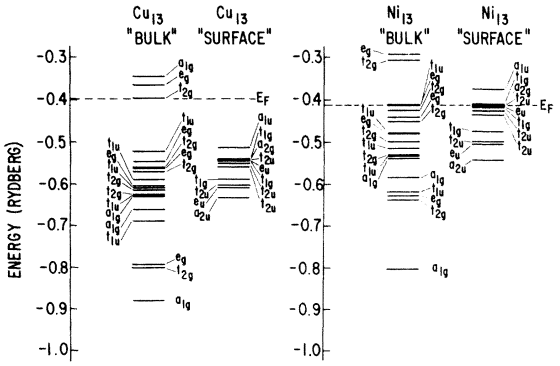

FIG. 15. Separation of the SCF-$X\alpha$-SW electronic energy levels for Cu_{13} and Ni_{13} clusters into "bulk" and "surface" components.

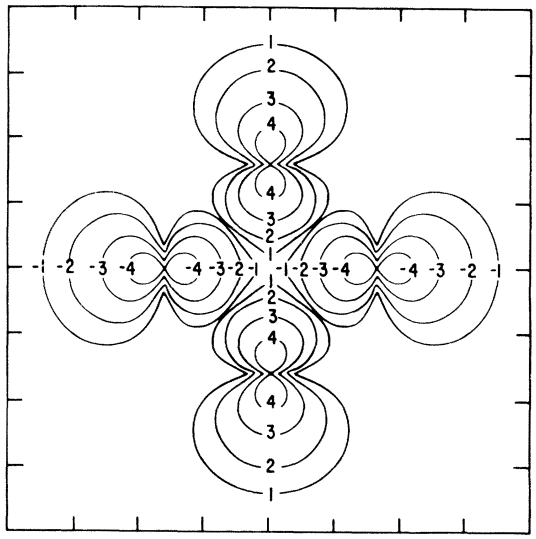

FIG. 16. Contour map for the occupied a_{2g} antibonding "surface" orbital of a Ni_{13} cluster, corresponding to the energy level -0.413 Ry shown in Fig. 15, plotted in the plane of the square face containing atoms 1–4 of the cubo-octahedron illustrated in Fig. 4.

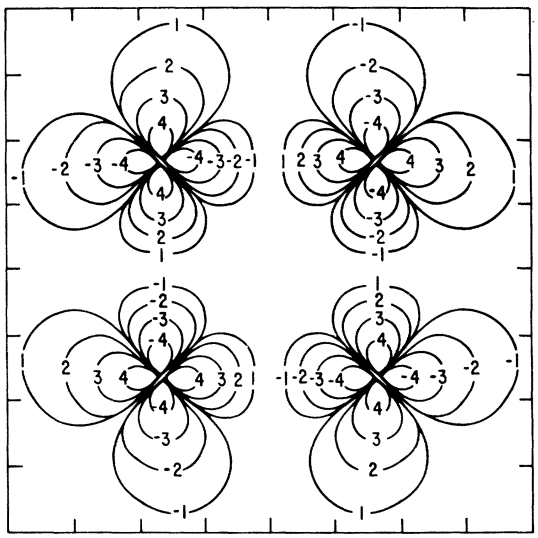

FIG. 17. Contour map for the occupied a_{2g} antibonding "surface" orbital of a Ni_{13} cluster, corresponding to the energy level -0.413 Ry shown in Fig. 15, plotted in the equatorial plane containing atoms 5–8, and 13 of the cubo-octahedron illustrated in Fig. 4.

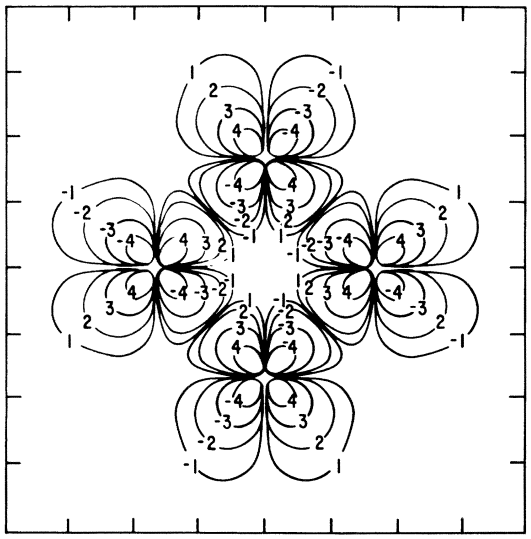

FIG. 18. Contour map for the unoccupied a_{1u} antibonding "surface" orbital of a Ni_{13} cluster, corresponding to the energy level -0.376 Ry shown in Fig. 15, plotted in the plane of the square face containing atoms 1–4 of the cubo-octahedron illustrated in Fig. 4.

of the cluster, as exemplified by the orbital contour maps shown in Figs. 16–18. In Figs. 16 and 17, respectively, the occupied a_{2g} orbital of Ni_{13} just below the Fermi level is mapped in a plane passing through the four nuclei (numbered 1–4 in Fig. 4) in a square face of the cubo-octahedron and in an equatorial plane containing four surface atoms and the central atom (numbered 5–8 and 13, respectively, in Fig. 4). The equatorial map in Fig. 17 clearly shows the absence of any contribution of the central atom to the wave function, consistent with the surface localization of the a_{2g} orbital.

The unoccupied Ni_{13} a_{1u} orbital lying above the Fermi level in Figs. 15 and 8 is mapped in Fig. 18 in the plane of a square face of the cubo-octahedron. The splitting off of this d orbital from the manifold of closely spaced d levels around the Fermi energy may be viewed, in the simplest approximation, as a "surface ligand-field" effect arising from the repulsion of neighboring surface atomic d orbitals. The empty a_{1u} d orbital also occurs in Pd_{13} and Pt_{13}, with the energy gap between this level and the Fermi level increasing through the series Ni_{13}, Pd_{13}, and Pt_{13} (cf. Figs. 8–10). In the case of Pd_{13}, the a_{1u} level is nearly degenerate with an empty s,p-like t_{1u} level. In Cu_{13}, the a_{1u} orbital is fully occupied and lies well below the Fermi energy (cf. Fig. 5). Because it is an empty "surface state" which is spatially oriented away from the surface in all three transition-metal clusters, it can overlap and effectively accept electrons from interacting adsorbate atoms and molecules. Such interactions and their possible relationship to catalytic activity and selectivity will be the subject of a future publication.[49]

One of the most significant results of these SCF-$X\alpha$ cluster calculations is the difference between the charge distribution of the surface atoms and that of the central atom obtained at self-consistency. The effective charges on the surface and central atoms of the Cu_{13}, Ni_{13}, Pd_{13}, and Pt_{13} clusters are summarized in Table III, based on counting the total number of electrons in the various regions of the clusters. These calculations suggest a slight depletion of electronic charge, i.e., a net positive charge, at the surface of each cluster, compensating for the electronic charge which is drawn toward the central atom. This result is expected, more or less, because the potential well associated with the central atom in the field of the 12 surrounding nuclei is deeper, and therefore more attractive, than the potentials of the surface atoms, which have lower coordination number. The small effective positive charges on the surface atoms of the cluster will tend to polarize or attract the electron charge clouds of approaching atoms or molecules, enhancing the overlap of highly directed cluster orbitals like those shown in Figs. 16–18 with the adsorbate orbitals and thereby promoting their interaction with the cluster.

As suggested in Sec. III B, the splitting off of the lowest t_{2g} and e_g energy levels from the bottom of the manifold of d levels in Cu_{13}, Ni_{13}, Pd_{13}, and Pt_{13} (cf. Figs. 5 and 8–11) is also an artifact of the deeper potential well of the central atom relative to the surface atoms. The spatial localization of these t_{2g} and e_g orbitals primarily on the central atom is evident in the wave-function contour maps for Cu_{13} shown in Figs. 6 and 7, respectively. Note in particular how the e_g d lobes in Fig. 7 are pointed toward the "surface" interstitial regions which correspond to the centers of the

TABLE III. Total numbers of electrons Q in atomic, interatomic, and extramolecular regions of the cubo-octahedral metal clusters, and the effective charges Δq on the central and surface atoms of the clusters.

	Cu_{13}	Ni_{13}	Pd_{13}	Pt_{13}
Q (central atom)	28.820	27.977	45.910	77.825
Q (surface atom)	28.132	27.070	45.022	76.767
Q (interatomic)	9.079	9.928	10.900	14.447
Q (extramolecular)	1.519	1.253	0.925	0.523
Δq[a] (central atom)	−0.518	−0.741	−0.748	−0.936
Δq[a] (surface atom)	+0.043	+0.062	+0.062	+0.078

[a]These quantities are determined by weighting the contributions of all 13 atoms to the interatomic region equally.

square faces of the cubo-octahedron (see Fig. 4). This implies that the wave functions of an adsorbate atom approaching the center of a square face could overlap the e_g orbital and thereby interact with the central atom. Although the 13-atom cubo-octahedral cluster is a very special case, the differences in potentials and charge distributions of the surface and central atoms are likely to have their counterparts in the surface and underlying layers of much larger aggregates. Thus chemisorption on such aggregates is likely to involve interactions of the adsorbate with both the surface and underlying substrate atoms, possibly leading to some penetration of the adsorbate into the cluster interstitial regions.[50]

Since the 13-atom cubo-octahedron is the simplest globular analog of the first two layers of a faceted or "stepped" fcc crystalline surface, one might expect the surface atoms, particularly those with low coordination number at the "corners" and "edges" of the facets, to have small effective positive charges relative to the underlying substrate atoms. How this property may be related to the observed sensitivity of catalytic activity to surface morphology[47] is currently under investigation.

Another possible application of the present cluster results is in regard to the interpretation of ultraviolet photoemission spectroscropy (UPS) data for crystalline transition metals.[45,46] For example, the optical d-band density of states for crystalline nickel as inferred from UPS measurements[45] is considerably narrower than the density of states predicted from bulk band-structure calculations.[32] This has been attributed to the fact that 20–40-eV photons in UPS measurements sample only two or three surface layers of the crystal, where the d-band density of states is estimated to be narrower than the ideal bulk bandwidth.[42] On the contrary, the width of the two principal peaks in the density of states for the Ni_{13} cluster shown in Fig. 13 is in relatively good agreement with the UPS data. Furthermore, the paramagnetic spin polarization of the Ni_{13} levels as displayed in Fig. 11 is consistent with the persistence of spin polarization in the UPS data above the Curie temperature and with the exchange splitting estimated from that data.[51] We find equally good agreement between the principal peaks in the densities of states for Cu_{13}, Pd_{13}, and Pt_{13} and UPS data for the corresponding crystalline surfaces.[45] These results suggest that a "localized" description of d-electron bonding, as provided by SCF-$X\alpha$ MO calculations for small clusters, may be a more realistic representation of the initial states of d-band photoelectron emission from the surface layers of a transition-metal crystal, than the delocalized Bloch representation of bulk band-structure theory.

Many of the above conjectures concerning the relevance of cluster electronic structure to surface electronic structure could be further tested by constructing theoretical models based on two-dimensional layers of atoms simulating the surfaces of ideal single crystals. One way of accomplishing this within the framework of finite cubo-octahedral clusters is to remove certain atoms from the cluster so that the central atom has the nearest-neighbor environment exclusively of an atom near the (100), (110), or (111) surface plane of an fcc crystal. SCF-$X\alpha$-SW calculations for such clusters are in progress. Theoretical formalisms and computational procedures, analogous to the SCF-$X\alpha$-SW approach to finite clusters, have recently been proposed for treating infinite two-dimensional layers of atoms and thin films.[52,53] Non-self-consistent results obtained for a monolayer of copper atoms[53] are too preliminary to justify comparison with the self-consistent Cu_{13} results presented in this paper.

V. COMPARISON OF EH, CNDO, AND SCF-$X\alpha$-SW METHODS FOR TRANSITION- AND NOBLE-METAL CLUSTERS

A. Extended-Hückel calculations

Recently a number of papers have appeared in which the extended-Hückel (EH) method has been used to investigate the electronic structure of transition- or noble-metal clusters[6,11–15] and the interaction of these clusters with adsorbates.[12–15] It had also been used previously to investigate adsorbate-substrate interactions in a nommetallic system.[10] A number of problems and shortcomings of the EH method for treating metal clusters[12] and chemisorption systems[10] have been recognized and discussed. One major problem is the proper treatment of electron transfer in a self-consistent manner. Another is the determination of the necessary parameters to treat transition metals.

In the general context of using clusters of metal atoms to represent substrates for chemisorption and catalysis studies, the question arises: how many atoms are needed to give a reasonable representation of the electronic structure of the true substrate? In the present section we will compare the answers provided by calculations made to date using the EH and SCF-$X\alpha$-SW methods.

It is well known that the SCF-$X\alpha$-SW method reduces to the KKR method[35] of band theory when applied to the perfect bulk metal[17] and that the latter has been very successfully used to describe the electronic structure of many metals.[4,5,30,34] Hence the SCF-$X\alpha$-SW method should provide a useful starting point for the investigation of finite metal clusters in an attempt to answer the above question. On the other hand, the extended-Hückel method has

not been successfully used to calculate the band structure of a transition metal and hence its efficacy for treating transition-metal clusters is *a priori* in doubt, even though the utility of the EH method for calculating the band structures of certain semiconductors as well as the electronic structures of finite clusters of atoms representing these semiconductors is well established.[54]

In recent EH calculations by Anderson and Hoffmann[15] (AH) for clusters simulating transition-metal surfaces and chemisorption thereon, charge differences of over one electron occur on neighboring atoms in some of the metal clusters. AH note that, although the charge buildups on atoms are overestimated owing to the approximate nature of the EH calculations, "*the sign and relative magnitude of the charges are nevertheless useful for qualitative discussion.*" Other workers such as Fassaert *et al.*[11] do not attribute any significance to the initial charges of the atoms in the metal cluster, but only consider changes in charge distribution relative to the isolated metal cluster in discussing chemisorption.

We have repeated the EH calculations for Ni_9 and W_9 and reproduced the results of AH.[15] Moreover we have extended the calculations (using the AH parameters) to clusters of W_{13} and Ni_{13}. For the latter cluster we may make a direct comparison with results obtained by the SCF-$X\alpha$-SW method. In the first four rows of Table IV the EH net atomic charge results are presented for the W_9, Ni_9, W_{13}, and Ni_{13} clusters using the AH parameters. The calculated charges for Ni_{13} are of the same sign as those found from the SCF-$X\alpha$-SW calculations (see Table IV). The energy levels which will be discussed below are not, however, in very good agreement. One thing which stands out immediately when comparing the first four rows of Table IV is the rather notable qualitative differences between the tungsten and nickel results. Such differences in charges according to AH[15] should be physically meaningful, if not in a quantitative sense, nevertheless, for qualitative discussion.

TABLE IV. Extended-Hückel net atomic charges for W and Ni clusters.[a]

Method	Cluster	Center atom	In-plane atoms[b]	Out-of-plane atoms[c]
AH	W_9	+0.74	+0.41	−0.59
AH	W_{13}	+1.52	−0.39	+0.39
AH	Ni_9	−0.25	−0.11	+0.17
AH	Ni_{13}	−0.17	+0.01	+0.01
SZAH	Ni_9	+0.38	+0.20	−0.30
SZAH	Ni_{13}	+2.73	−0.23	−0.23
FVA	Ni_{13}	+2.54	−0.21	−0.21

[a] Clusters for W and Ni have somewhat different geometries because W has a bcc structure and Ni is an fcc structure.

[b] Four atoms which are in the same plane as the center atom.

[c] Four (or eight) atoms which are in the plane(s) above (and below) the plane containing the center atom.

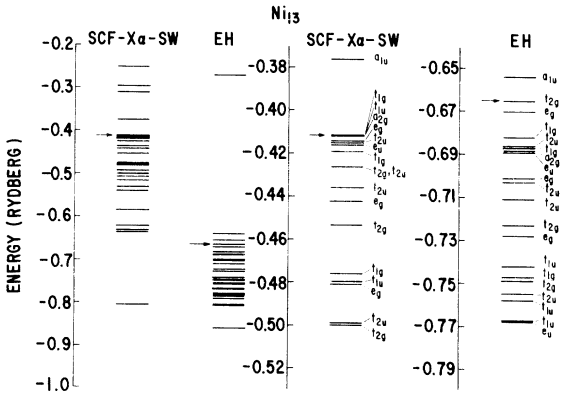

FIG. 19. Comparison of the electronic energy levels of a cubo-octahedral Ni_{13} cluster as determined by the spin-restricted SCF-$X\alpha$-SW and extended-Hückel (EH) methods. Highest occupied orbitals are indicated by arrows.

There is, however, an anomalous difference in basis functions between the AH calculations for tungsten and nickel. In the former case a single Slater function (single ξ, SZ) is used to represent the d orbital, whereas for nickel a double ξ function is used. When the Ni_9 and Ni_{13} calculations are repeated using a SZ function for Ni ($\xi = 2.0$) and keeping all other AH parameters the same, which is comparable to the AH tungsten calculations, a rather different charge distribution is obtained (see Table IV). In comparing rows 3 and 4 with 5 and 6 of the table, we find that the net charges change not only in magnitude but also in sign and that the SZ AH results are qualitatively similar to the single ξ results of AH for tungsten. Thus we are led to the conclusion that the large differences in net charges in the AH results between Ni and W clusters are *not physically significant but reflect differences in parametrization*. This is further supported by the results of Fassaert, Verbeek, and van der Avoird[11] for a Ni_{13} cluster using the EH method, but with a different parametrization. The resultant charges are given in the seventh row of Table IV and labeled FVA.

In Fig. 19 a comparison is provided for the one-electron energies obtained from the SCF-$X\alpha$-SW and EH calculations. The EH calculations shown are for the AH parameters. To the left all the occupied valence levels are shown, to the right the higher occupied levels are shown on an enlarged scale. The comparison between the two calculations shows rather little agreement.

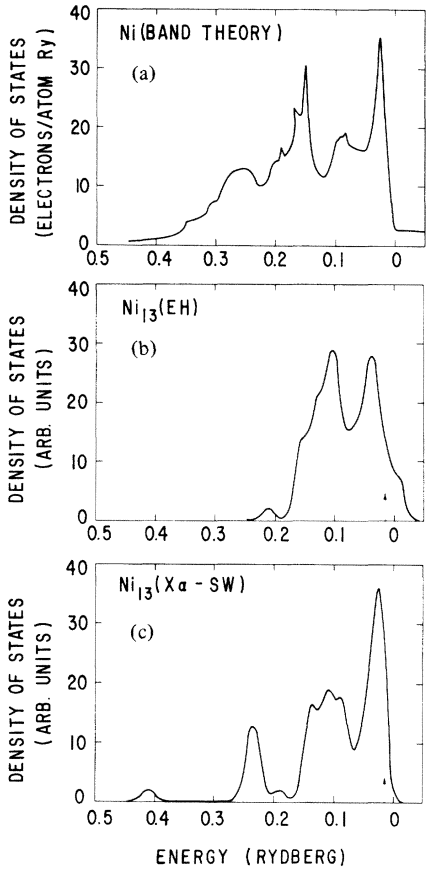

FIG. 20. Comparison of the electronic density of nickel as determined from : (a) a bulk band-structure calculation (Ref. 32), (b) a cubo-octahedral Ni_{13} cluster using the extended-Hückel (EH) method, and (c) a cubo-octahedral Ni_{13} cluster using the SCF-$X\alpha$-SW method.

Returning to the question posed earlier of how well a small cluster represents the electronic structure of a crystalline metal, it is convenient to present the results of Fig. 19 in the form of densities of states (DOS), as was done in Sec. IV A, to compare with the DOS of bulk nickel. Namely, we calculate the DOS for the Ni_{13} cluster by replacing each discrete eigenvalue (see Fig. 19) by a Gaussian with a width of 0.01 Ry, weighted by the degeneracy of the orbital. The result is shown in Fig. 20 where it is compared to the DOS results from the SCF-$X\alpha$-LCAO band structure of Callaway and Wang[32] for bulk Ni. As the extended-Hückel method is a spin-restricted procedure here we compare only the SCF-$X\alpha$-SW spin-restricted results and likewise use only the majority-spin DOS results of Callaway and Wang rather than their total spin-unrestricted results. It is clear from Fig. 20 that the EH and SCF-$X\alpha$-SW DOS for Ni_{13} are quite different and that the SCF-$X\alpha$-SW results have many features in common with the crystalline DOS (allowing for the effects of the cluster surface discussed in Sec. IV B), whereas this is not the case for the EH results.

In Secs. III B and IV A we have described the SCF-$X\alpha$-SW results for Cu_{13}, Pd_{13}, and Pt_{13} clusters along with the results for Ni_{13}. It is therefore of interest here to compare some results of these calculations for Cu_{13} and Pd_{13} with recent EH calculations for Cu and Pd clusters by Baetzold and Mack.[6] Experimentally it is known that the d bandwidth increases through the series Cu, Ni, Pd, and Pt.[38] As we have shown in Sec. IV A, this trend is reproduced by the SCF-$X\alpha$-SW calculations for 13-atom clusters. The results for even larger clusters, i.e., 19 atoms, by Baetzold and Mack[6] using the EH method give results for Cu and Pd which are inconsistent with experiment and with the Ni results using the AH parameters. Baetzold and Mack calculate d bandwidths for Cu_{19} and Pd_{19} of ~0.2 and 0.3 eV, respectively (cf. Fig. 9 of Baetzold and Mack's[6] paper), whereas the experimental d bandwidths as well as those calculated by the SCF-$X\alpha$-SW method are of the order of several eV. Baetzold and Mack state: "In most properties, the clusters in the size range reported here are different from the bulk metals." Hence this seems to represent the answer to the questions posed above, as provided by extended-Hückel calculations. This conflicts, however, with the answer which emerges from SCF-$X\alpha$-SW calculations carried out thus far. These latter calculations suggest that much of the bulk bandwidth and DOS structure can be obtained with a cluster of approximately a dozen atoms.

We suggest that this discrepancy arises from the EH calculations owing to the current arbitrariness in parametrizations[6,11,15] used for transition metals in this method. A possible systematic approach to the problem would be to obtain parameters by matching the occupied bands as obtained from an EH band-structure calculation of the metal with those obtained from more rigorous band calculations, in much the same spirit as previously used for semiconductors.[54] These parameters would then provide a reasonable starting point for calculating clusters of metal atoms. Alternatively, EH parameters might be chosen by matching to the results of SCF-$X\alpha$-SW calculations on clusters.

The importance of having a reasonable description of the electronic structure of a metal cluster, before using this cluster to study the chemisorption of molecules cannot be overemphasized. The inadequacy of the AH parametrization (as seen in Table IV and Fig. 20) must be a strong contributing factor, along with the effects of self-consistency in charge transfer, to the fact that the Anderson-Hoffmann[15] explanation of the photoemission results for CO chemisorbed on Ni is inconsistent with the most recent and definitive experimental data.[55]

B. CNDO calculations

The first calculations which attempted to determine the electronic properties of noble- and transition-metal clusters were reported in 1971 by Baetzold,[6] who used both extended-Hückel and CNDO methods to investigate silver and palladium clusters. The electronic structures of silver clusters containing up to 20 atoms were calculated by the EH method, but owing to the fact that the CNDO calculations are computationally more demanding, only clusters of up to eight atoms were considered in this case. Unfortunately, the author did not compare his distribution of energy levels with the total density of states (DOS) of the bulk solids as determined from an accurate band-structure calculation, which would have provided an immediate assessment of how closely the electronic structure of a small metal cluster resembles that of the bulk solid. The strictly energetic information obtained by a comparison to the bulk DOS of course can be supplemented by comparison of the atomic-orbital character of the cluster wave functions with the orbital character of the corresponding energy-band states. The author did discuss the effect of cluster size on the lowest ionization potential and on the binding energy per atom, finding for the Ag clusters that the ionization potential decreased toward the bulk value with larger clusters and that the binding energy per atom increased with cluster size, not however in a simple monotonic fashion.

More recently, Blyholder[9] has reported CNDO calculations for nickel clusters containing up to 13 atoms. The CNDO parameters were chosen by treating an octahedral Ni_6 cluster and trying to match selected quantities of the bulk such as the binding energy per atom, Fermi level, and d bandwidth. A distribution of the orbitals as a function of energy for a 13-atom cubo-octahedral cluster was presented and a discussion of the atomic character of the wave functions was given. Again, no direct comparison with bulk band structure or density of states was given.

In Fig. 21, we compare the DOS for Ni_{13} based on the CNDO results of Blyholder[9] with the DOS for bulk nickel based on the SCF-$X\alpha$-LCAO bandstructure results of Callaway and Wang.[32] Also included for comparison are the DOS resulting from the EH calculation for Ni_{13} using the Anderson-Hoffmann[15] parameters. In order to provide a meaningful comparison of the three calculations, the energy scales have been shifted so as to line up the bulk Fermi level with the highest occupied orbital of the clusters. For the CNDO calculation, we see that there is not a high density of states at the Fermi energy (E_F), in contrast to the results for bulk nickel, and that the high DOS in the CNDO results occurs at an energy for which the DOS in the bulk

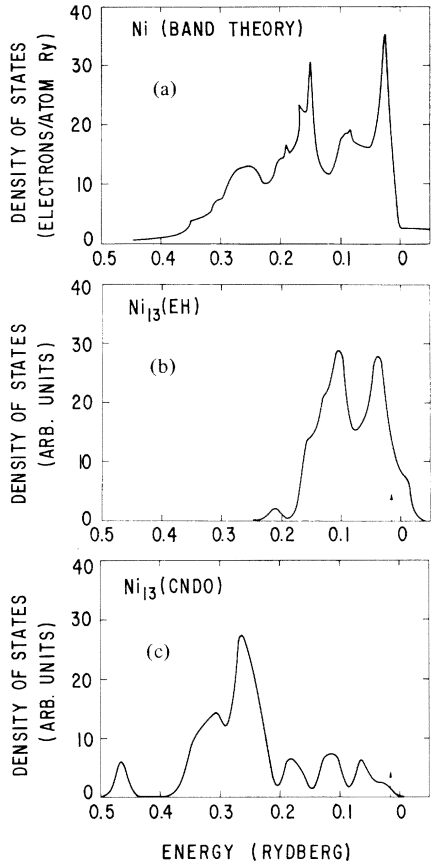

FIG. 21. Comparison of the electronic density of states of nickel as determined from: (a) a bulk band-structure calculation (Ref. 32), (b) a cubo-octahedral Ni_{13} cluster using the extended-Hückel (EH) method, and (c) a cubo-octahedral Ni_{13} cluster using the complete-neglect-of-differential-overlap (CNDO) method.

is rapidly decreasing. For the EH case, there is a high DOS near E_F but the d bandwidth is much narrower than in the bulk case, the s-d hybridization responsible for the long tail far from E_F in the bulk case is almost absent in the EH cluster calculation. The differences between the CNDO and EH calculations for Ni_{13} are quite significant.

VI. CONCLUSIONS

On the basis of the SCF-$X\alpha$-SW calculations presented in this paper, one is at first struck by the systematic similarities, rather than the differences, between the electronic structures of small transition- and noble-metal clusters and those of the corresponding crystalline metals. It is also clear that this observation cannot be made regarding the extended-Hückel and CNDO methods, and in fact the contrast between the SCF-$X\alpha$-SW results and these semiempirical LCAO calculations is rather profound in most cases.

On the other hand, the finite size of the clusters,

in particular the fact that most of the atoms are "surface" atoms, leads to some notable differences between the electronic structures of the clusters as calculated by the SCF-$X\alpha$-SW methods and those based purely on bulk band-structure considerations. For example, the splitting off of localized electronic states above and below the manifold of closely spaced d levels is observed for all the cubo-octahedral transition-metal clusters treated, and the energies of these states with respect to the Fermi level vary systematically through the elements Ni, Pd, and Pt. These states may be interpreted as the cluster analogs of surface states postulated for crystalline transition metals. Associated with the cluster surface states is an effective depletion of surface electronic charge, and hence net effective positive surface charge, compensated for by the building up of excess electronic charge around the central atom of the cluster. The high ionization potentials of the clusters (~7 eV) in comparison with the work functions of the corresponding crystalline metals (~5 eV) and the reduced paramagnetic magneton number of nickel clusters, as compared with bulk nickel, are also consequences of the small cluster size and large effective surface.

One frequently hears the statement that very small clusters of metal atoms are intrinsically "different" in their catalytic behavior from larger particles or single-crystal surfaces, especially in connection with so-called "demanding" or structure-sensitive reactions.[1,2] The much higher fraction of corner and edge atoms present at the surface of a small cluster (see Fig. 4) and the presence of spatially directed surface d orbitals at these corners and edges (see Fig. 18) could contribute to the structure sensitivity of such catalytic reactions through the preferential chemisorption of reacting molecules at these sites. Furthermore, the effective positive charge of the surface atoms and concomitant electric field could enhance the interaction of the reacting molecules through charge polarization or transfer. Other things being equal, the relatively large work function and high electronic affinity of a small metal cluster would also tend to favor charge transfer from a nucleophilic adsorbate to the cluster.

In regard to the nature of chemisorption on cluster surfaces, it is important to note the occurrence in inorganic chemistry of metal cluster compounds,[56] such as the one illustrated in Fig. 22. This is an example of a molecular cluster on which linear and bridged carbonyl groups are formed, both of which have been speculated to form in the chemisorption of CO on metal surfaces. The existence of such complexes suggests how a very small metal cluster can form more or less normal sorts of chemical bonds on the cluster surface and particularly at corners and edges.

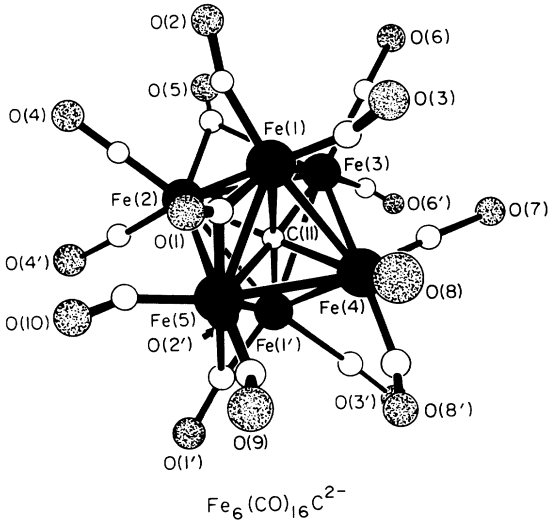

FIG. 22. Structure of the iron carbonyl carbide molecular ion, $Fe_6(CO)_{16}C^{2-}$ (see Ref. 60).

One can systematically study the chemisorption of atoms and molecules on the surfaces of clusters of the type considered in this paper, using the SCF-$X\alpha$-SW method, and such calculations are currently in progress. It should be pointed out, of course, that the transition- and noble-metal clusters treated in this paper are of rather limited size and geometry. Indeed, these geometries may not be the most stable ones for small metal clusters. For example, earlier SCF-$X\alpha$-SW calculations for lithium clusters indicated that a 13-atom icosahedral structure is preferred over a 13-atom cubo-octahedral one.[22] Calculations for icosahedral transition-metal clusters are now in progress. Furthermore, Jahn-Teller effects and the interactions of adsorbates with metal clusters could influence their geometries.

When utilized as the active centers of a heterogeneous catalyst, small metal clusters are usually supported in a porous refractory material such as silica or alumina.[3] If the structure sensitivity of catalytic reactions cannot be explained solely in terms of the surface morphology of the clusters themselves, then it is possible that the supporting material itself may be involved.[1] Most supporting materials are oxides and may act to withdraw electrons from the small metal clusters in contact with them, much in the same way as the ligands of a simple transition-metal complex withdraw electrons from the transition-metal atom. The electron depletion could then allow the small metal cluster to interact with adsorbates in a different manner from the elemental clusters themselves. On the other hand, for larger metal aggregates or

particles in a support, the electron withdrawing effect of the surrounding material may be largely screened out by the intervening metal atoms, from the surface of the particle. Thus for these larger particles the main effect on catalytic behavior might be determined by the effective surface area.

For example, clusters of less than six platinum atoms small enough to be contained in the supercages of a *Y* zeolite exhibit an anomalously high catalytic activity for reactions of hydrogenation, isomerization, and hydrogenolysis.[57] They also chemisorb less oxygen than larger platinum crystallites. This fact and the enhanced catalytic activity have been attributed to electron transfer from the small platinum clusters to the zeolite support, as if platinum were behaving more like its neighbor, iridium, to the left in the periodic table.[57]

It is possible to construct realistic theoretical models for the effects of supporting materials on the electronic structure of a small metal cluster by embedding the cluster in a matrix simulating the local molecular environment of the support, and then carrying out SCF-$X\alpha$-SW calculations for the composite system. The electronic structure and chemisorption capacity of the composite system can then be compared with the results calculated for the isolated metal cluster. Such calculations are now in progress.

Related to this problem is a recent SCF-$X\alpha$-SW calculation by Yang *et al.*[58] on a model for the active sites of ferredoxin, an iron-sulfur protein which acts as an electron-transfer agent in the metabolism of bacteria, plants, and animals. The active site, an $[Fe_4S_4(S\text{-cys})_4]$ cluster, consists of a somewhat distorted cube of Fe and S atoms on alternate vertices, with four outer sulfur atoms attaching the cluster to the surrounding protein via cysteinyl moieties. The sulfur atoms and cysteinyl groups may be viewed as providing a "support" for the Fe_4 cluster, and therefore possible analogies with the effects described above are obvious. Indeed, the results of the SCF-$X\alpha$-SW calculations for ferredoxin suggest significant amounts of charge transfer and orbital delocalization of the Fe_4 electrons onto the surrounding sulfur ligands, in good agreement with all available experimental data. There are probably many useful analogies to be made among the active centers of heterogeneous catalysts, transition-metal complexes, and proteins and enzymes containing transition-metal atoms. Such analogies are probably *not* fortuitous. They should be sought after and the common basis for understanding elucidated.

Very small "alloyed" particles in the form of supported bimetallic and multimetallic clusters have also become increasingly important in heterogeneous catalysis, particularly in the design of catalysts that are selective for specific reactions.[59] With the SCF-$X\alpha$-SW technique, it is possible to model the effects of alloying on the electronic structure and chemisorption capacity of a small metal cluster by systematically carrying out the calculations for the composite cluster as a function of composition. Calculations on Cu-Ni clusters are in progress.

ACKNOWLEDGMENTS

One of us (R. P. M.) is grateful to the AFOSR, Contract No. F44620-72-C-0008, for supporting phases of this research carried out at General Electric. One of us (K. H. J.) gratefully acknowledges support provided by the NSF and Petroleum Research Fund (administered by the American Chemical Society) for phases of this research carried out at M. I. T. relevant to the electronic structures and properties of heterogeneous catalysts. Support for those aspects of this research at M. I. T. relevant to the electronic structures of transition-metal surfaces is provided by the ONR under Contract No. N00014-75-C-0970. Supplementary support for computation costs at M. I. T. was provided by the Shell Companies Foundation. We are grateful to Professor M. Boudart and Professor W. Spicer of Stanford University and to Dr. T. E. Fischer, Dr. C. R. Helms, and Dr. J. H. Sinfelt of Exxon Research and Engineering Company for valuable discussions.

---

*Present address: Florida Technological University, Orlando, Fla.

†Present address: The University of Pittsburgh at Bradford, Bradford, Penn.

[1]M. Boudart, in *Proceedings of the Robert A. Welch Foundation Conference on Chemical Research. XIV Solid State Chemistry*, edited by W. O. Milligan (The Robert A. Welch Foundation, Houston, Texas, 1970), p. 299.

[2]J. H. Sinfelt, in *Annual Review of Materials Science*, edited by R. A. Huggins, R. H. Bube, and R. W. Roberts (Annual Reviews, Palo Alto, California, 1972), Vol. 2, p. 641.

[3]J. R. Anderson, *Structure of Metallic Catalysts* (Academic, New York, 1975).

[4]*Energy Bands in Metals and Alloys*, edited by L. H. Bennett and J. T. Waber (Gordon and Breach, New York, 1968).

[5]*Electronic Density of States*, edited by L. H. Bennett (National Bureau of Standards Spec. Pub. 323, Washington, D. C., 1971).

[6]R. C. Baetzold, J. Chem. Phys. 55, 4363 (1971); J. Catal. 29, 129 (1973); R. C. Baetzold and R. E. Mack, J. Chem. Phys. 62, 1513 (1975).

[7]M. Wolfsberg and L. Helmholz, J. Chem. Phys. 20, 837 (1953); R. Hoffmann, *ibid.* 39, 1397 (1963).

[8]J. A. Pople and D. L. Beveridge, *Approximate Molecular Orbital Theory* (McGraw-Hill, New York, 1970).

[9]G. Blyholder, Surf. Sci. 42, 249 (1974).
[10]A. J. Bennett, B. McCarroll, and R. P. Messmer, Surf. Sci. 24, 191 (1971); Phys. Rev. B 3, 1397 (1971).
[11]D. J. M. Fassaert, H. Verbeek, and A. van der Avoird, Surf. Sci. 29, 501 (1972).
[12]L. W. Anders, R. S. Hansen, and L. S. Bartell, J. Chem. Phys. 59, 5277 (1973).
[13]L. W. Anders, R. S. Hansen, and L. S. Bartell, J. Chem. Phys. 62, 1641 (1975).
[14]J. C. Robertson and C. W. Wilmsen, J. Vac. Sci. Technol. 9, 901 (1972).
[15]A. B. Anderson and R. Hoffmann, J. Chem. Phys. 61, 4545 (1974).
[16]G. Blyholder, J. Chem. Phys. 62, 3193 (1975).
[17]J. C. Slater and K. H. Johnson, Phys. Rev. B 5, 844 (1972); K. H. Johnson and F. C. Smith, Jr., *ibid.* 5, 831 (1972).
[18]J. C. Slater, in *Advances in Quantum Chemistry*, edited by P.-O. Löwdin (Academic, New York, 1972), Vol. 6, p. 1; J. C. Slater, *Quantum Theory of Molecules and Solids* (McGraw-Hill, New York, 1974), Vol. 4.
[19]K. H. Johnson, J. Chem. Phys. 45, 3085 (1966); in *Advances in Quantum Chemistry*, edited by P.-O. Löwdin (Academic, New York, 1973), Vol. 7. p. 143.
[20]K. H. Johnson, J. G. Norman, Jr., and J. W. D. Connolly, in *Computational Methods for Large Molecules and Localized States in Solids*, edited by F. Herman, A. D. McLean, and R. K. Nesbet (Plenum, New York, 1973), p. 161.
[21]K. H. Johnson, in *Annual Review of Physical Chemistry*, edited by H. Eyring, C. J. Christensen, and H. S. Johnston (Annual Reviews, Palo Alto, California, 1975), Vol. 26, p. 39.
[22]J. G. Fripiat, K. T. Chow, M. Boudart, J. B. Diamond, and K. H. Johnson, J. Molec. Catal. (to be published).
[23]J. C. Slater and K. H. Johnson, Phys. Today 27, 34 (1974).
[24]R. P. Messmer, in *The Physical Basis of Heterogeneous Catalysis*, edited by R. I. Jaffe and E. Drauglis (Plenum, New York, 1975).
[25]R. P. Messmer, in *Modern Theoretical Chemistry*, edited by G. A. Segal (Plenum, New York, 1976, Vol. 4.
[26]R. P. Messmer, C. W. Tucker, Jr., and K. H. Johnson, Chem. Phys. Lett. 36, 423 (1975).
[27]F. Herman, A. R. Williams, and K. H. Johnson, J. Chem. Phys. 61, 3508 (1974).
[28]J. G. Norman, Jr., J. Chem. Phys. 61, 4630 (1974).
[29]M. Boudart, LSAC Internal Reports Nos. 4 and 6 (Stanford University, 1972) (unpublished).
[30]B. Segall, Phys. Rev. 125, 109 (1962); G. A. Burdick, Phys. Rev. 129, 138 (1963).
[31]H. Ehrenreich and H. R. Phillipp, Phys. Rev. 128, 1622 (1962).
[32]J. Callaway and C. S. Wang, Phys. Rev. B 7, 1096 (1973).
[33]J. L. Carter and J. H. Sinfelt, J. Catal. 10, 134 (1968).
[34]J. F. Janak, A. R. Williams, and V. L. Moruzzi, Phys. Rev. B 11, 1522 (1975).
[35]J. Korringa, Physica (Utr.) 13, 392 (1947); W. Kohn and N. Rostoker, Phys. Rev. 94, 1111 (1954).
[36]D. House and P. V. Smith, J. Phys. F 3, 753 (1973).
[37]J. Keller and R. Jones, J. Phys. F 1, L33 (1971).
[38]C. S. Fadley and D. A. Shirley, J. Res. Natl. Bur. Stand. (U.S.) A 74, 543 (1970); Y. Baer, F.-F. Hedén, J. Hedman, M. Klasson, C. Nordling, and K. Siegbahn, Phys. Scripta 1, 55 (1970).
[39]S. G. Davison and J. D. Levine, in *Solid State Physics*, edited by H. Ehrenreich, F. Seitz, and D. Turnbull, (Academic, New York, 1970), Vol. 25, p. 1.
[40]R. O. Jones, in *Surface Physics of Semiconductors and Phosphors*, edited by C. A. Scott and C. E. Reed (Academic, New York, 1973).
[41]F. Forstmann and V. Heine, Phys. Rev. Lett. 24, 1419 (1970).
[42]R. Haydock, V. Heine, M. J. Kelly, and J. B. Pendry, Phys. Rev. Lett. 29, 868 (1972).
[43]S. J. Gurman and J. B. Pendry, Phys. Rev. Lett. 31, 637 (1973).
[44]G. S. Painter, P. J. Jennings, and R. O. Jones, J. Phys. C 8, L199 (1975).
[45]D. E. Eastman, in *Electron Spectroscopy*, edited by D. A. Shirley (North-Holland, Amsterdam, 1972), p. 487.
[46]F. Feuerbacher and B. Fitton, Phys. Rev. Lett. 30, 923 (1973).
[47]S. L. Bernasek, W. J. Siekhaus, and G. A. Somorjai, Phys. Rev. Lett. 30, 1202 (1973).
[48]K. H. Johnson and G. Hochstrasser, in *The Physical Basis of Heterogeneous Catalysis*, edited by R. I. Jaffee and E. Drauglis (Plenum, New York, 1975).
[49]K. H. Johnson and R. P. Messmer (unpublished).
[50]R. P. Messmer, C. W. Tucker, Jr., and K. H. Johnson, Surf. Sci. 42, 341 (1974).
[51]D. T. Pierce, Technical Report No. 5227-2 (Solid State Laboratory, Stanford Electronics Laboratories, Stanford University, Stanford, Cal., 1970) (unpublished); D. T. Pierce and W. E. Spicer, Phys. Rev. Lett. 25, 581 (1970).
[52]W. Kohn, Phys. Rev. B 11, 3756 (1975).
[53]N. Kar and P. Soven, Phys. Rev. B 11, 3761 (1975).
[54]R. P. Messmer, Chem. Phys. Lett. 11, 589 (1971); G. D. Watkins and R. P. Messmer, in *Computational Methods for Large Molecules and Localized States in Solids*, edited by F. Herman, A. D. McLean, and R. K. Nesbet (Plenum, New York, 1973), p. 133; R. P. Messmer and G. D. Watkins, Phys. Rev. B 7, 2568 (1973); C. Weigel, R. P. Messmer, and J. W. Corbett, Phys. Status Solidi B 57, 455 (1973).
[55]T. Gustafsson, E. W. Plummer, D. E. Eastman, and J. L. Freeouf, Solid State Commun. 17, 391 (1975).
[56]F. A. Cotton, Q. Rev. Chem. Soc. 20, 389 (1966); Acc. Chem. Res. 2, 240 (1969).
[57]R. A. Dalla Betta and M. Boudart, in *Proceedings of the Fifth International Congress on Catalysis*, edited by J. W. Hightower (North-Holland, Amsterdam, 1973), p. 1329.
[58]C. Y. Yang, K. H. Johnson, R. H. Holm, and J. G. Norman, Jr., J. Amer. Chem. Soc. 97, 6596 (1975).
[59]J. H. Sinfelt, J. Catal. 29, 308 (1973).
[60]M. R. Churchill, J. Wormwald, J. Knight, and M. J. Mays, J. Amer. Chem. Soc. 93, 3073 (1971).